OPTIMISED CONTROL OF A HYBRID BOOST CONVERTER FOR A PV CHARGING STATION USING PARTICLE SWARM TECHNIQUE

[1]Kavali Babitha,[2]Dr.G.S.Durga Prasad,[3]K.Giri Babu
[1]PG Student,[2]Professor,[3]Assistant Professor
[1,2,3]Department of Electrical and Electronic Engineering,
[1,2,3]J.B.Institute of Engineering and Technology, Hyderabad.

Abstract: Hybrid Boost Converter (HBC) has been proposed to act as DC/DC converter as well as DC/AC converter to reduce switching losses and conversion stages. In this paper, the system consists of a PV system, a HBC, Plug-in Hybrid Electric Vehicle (PHEV) and AC system. The Particle Swarm Optimization (PSO)–MPPT algorithm is implemented to extract more power from PV array. MPPT , PLL and Vector control are the control schemes used to control the performance of HBC. It is designed to realize Maximum Power Point Tracking (MPPT) and power management. A testbed with power electronics switching details is built in MATLAB/SimPowersystems for validation. Simulation results demonstrate the feasibility of designed control architecture.

Index Terms **– Hybird Boost Converter (HBC) , Plug-in Hybrid Electric Vehicle (PHEV) , Photovoltaic (PV) , Maximum Power Point Tracking (MPPT), Particle Swarm optimization(PSO).**

I. INTRODUCTION

The environmental and economic advantages of PHEV lead to the increase in number of production and consumption [2]. The U.S. Department of Energy forecasts that over one million PHEVs will be sold in the U.S. during the next decade [3]. Research has been conducted on developing a charging station by integrating a three-phase ac grid with PHEVs [4]–[6]. The comparison of different PHEV chargers' topologies and techniques are reviewed in [2], [7]. However, a large-scale penetration of PHEVs may add more pressure on the grid during charging periods. Therefore, charging stations with PV as an additional power source become a feasible solution.

The objective of the paper is to implement such a multi-port converter in a PV charging station for PHEVs and design the controller.

II. THREE-PHASE HBC- BASED PV CHARGING STATION TOPOLOGY AND OPERATION

A three-phase HBC uses the same amount of switches as a two-level voltage source converter (VSC). However, the HBC can realize both dc/dc conversion and dc/ac conversion. As a comparison, Fig.2.1 shows the conventional PV charging station where a dc/dc boost converter and a three-phase VSC are used to integrate the PV system, the PHEVs and the ac grid. A three-phase HBC replaces the two converters: the dc/dc boost converter and the dc/ac three-phase VSC to decrease the energy conversion stages and the power losses of the PV charging station. Fig.2.2 shows the HBC-based PV charging station's topology. The main components of the configuration of the PV charging station consist of PV array, three-phase bidirectional HBC, ac grid, off-board dc/dc converter, and PHEV's batteries.

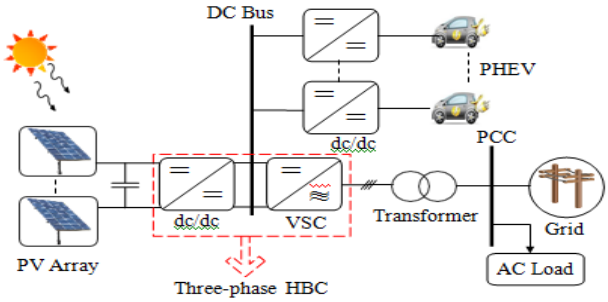

Figure 2.1 Architecture configurations of a PV charging station.

The system is composed of a PV array, a dc system, a three-phase ac system, and the interfacing three-phase HBC as shown in Fig.2.2. The PV side includes a large inductance to achieve continuous condition and capacitance to decrease the voltage ripple. The dc side includes a diode, a dc bus for PHEV connection, a dc capacitor to eliminate the output current ripples, an off-board unidirectional isolated dc/dc converter, and PHEV batteries. The ac system includes a three-phase LC filter, a step-up transformer, and the point of common coupling (PCC) bus that connects the PV station to the main grid.

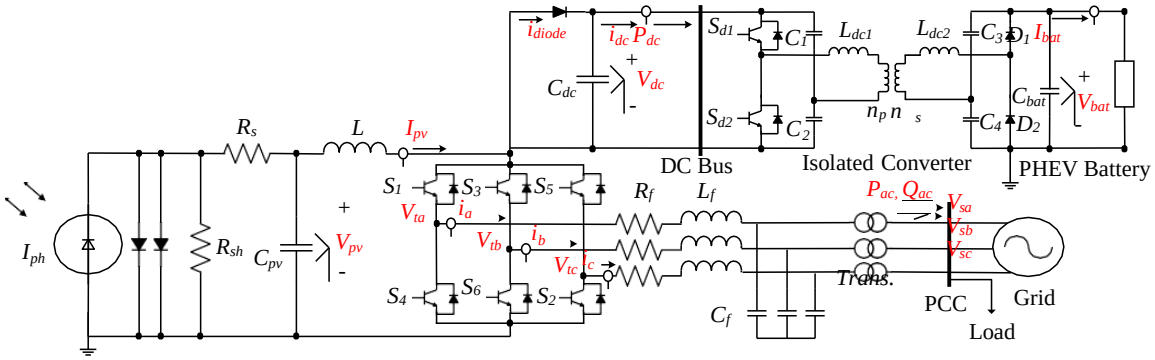

Figure 2.2 Topology of the three-phase HBC-based PV charging station.

Traditional dc/dc boost converter is operated on two modes which are "on" and "off" states. Conventional VSC is operated on "active" and "zero" modes where the output ac power can have a value or zero. The three-phase HBC integrates the operational phases of a VSC and a dc/dc converter into three main modes. The main three intervals include a shoot-through (ST) mode, an active mode (A), and a zero mode (Z).

$$\mathrm{Vdc} = \frac{\mathrm{Vpv}}{1-\mathrm{Dst}} \ , \mathrm{Vac} = \mathrm{Mi}\frac{\mathrm{Vdc}}{2} \tag{2.1}$$

$$VLL = Mi\frac{\sqrt{3}\,Vdc}{2\sqrt{2}} = 0.612\frac{Mi}{1-Dst}\,Vpv \tag{2.2}$$

where M_i and D_{st} are the ac voltage per-phase modulation index and duty cycle of the shoot-through period, Vdc, Vac, and V_{LL} are the peak dc voltage, peak per-phase ac voltage, the RMS value of the line-to-line output ac voltage, respectively. It can be concluded from (2.2) that the dc output depends on only D_{st} while ac output depends on both D_{st} and M_i. In order to achieve continuous control of modified PWM, the controlling signals have to achieve this condition:

$$M_i + D_{st} < 1 \tag{2.3}$$

2.1 MODIFIED PWM

It is mentioned in Section II that the three-phase HBC is operated at three main intervals which are integrated between boost converter and VSC's phases. Conventional sinusoidal PWM and dc PWM are not appropriate to operate the switching states of three-phase HBC. Instead of separately controlling the dc and ac outputs using the switches of three- phase HBC, a modified PWM is applied to control two outputs at the same time. It is recommended to insert the shoot-through phase within the zero mode where the output ac power equals zero in this phase [21]. During the shoot-through period, one leg of the two switchings, e.g., S_1 and S_4 are both on. This leads to PV side current flowing into S_1, S_4 only. During the shoot-through period, the inductor L gets charged. At the zero mode, all upper-level switches S_1, S_3 and S_5 are on while the lower-level switches S_4, S_6 and S_2 are off. At this mode, the PV side current all flows to the dc side battery systems while the current to the ac system is zero. Finally, during the active mode, current will flow into the ac system.

Modified PWM regulates the switching states by controlling five signals which are three-phase ac signals V_a, V_b, V_c, and dc signals V_{st} ($V_{st} = 1 - D_{st}$), and $-V_{st}$. The ac controlling signals V_a,V_b, and V_c are controlled by modulation index Mi as well as phase angles while the dc signals $+V_{st}$ and $-V_{st}$ are regulated by duty ratio Dst. The advantage of using modified PWM is that both dc and ac outputs can be adjusted.

III. CONTROL OF PV CHARGING STATION

Three main control blocks are used to control the three- phase HBC: MPPT, phase-locked loop (PLL) and vector control as shown in Fig.3.1. Each block will be described by a subsection. The charging algorithm of the off-board isolated dc/dc converter will also be addressed in this section.

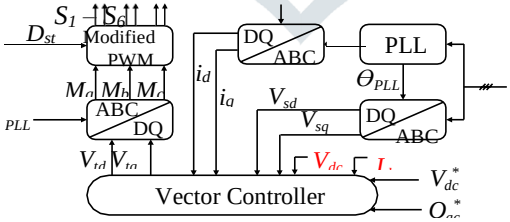

Figure 3.1 Control blocks of the HBC-based PV charging station.

3.1 PSO - MPPT

A basic variant of the PSO algorithm works by having a population (called a swarm) of candidate solutions (called particles). These particles are moved around in the search-space according to a few simple formulae. The movements of the particles are guided by their own best known position in the search-space as well as the entire swarm's best known position. When improved positions are being discovered these will then come to guide the movements of the swarm. The process is repeated and by doing so it is hoped, but not guaranteed, that a satisfactory solution will eventually be discovered.

Particle swarm optimization (PSO) algorithm is a stochastic optimization technique based on swarm, which was proposed by Eberhart and Kennedy (1995) and Kennedy and Eberhart(1995). PSO algorithm simulates animal's social behavior, including insects, herds, birds and fishes. These swarms conform a cooperative way to find food, and each member in the swarms keeps changing the search pattern according to the learning experiences of its own and other members. Main design idea of the PSO algorithm is closely related to two researches: One is evolutionary algorithm, just like evolutionary algorithm; PSO also uses a swarm mode which makes it to simultaneously search large region in the solution space of the optimized objective function. Million as proposed five basic principles (van den Bergh 2001):

(1) Proximity: the swarm should be able to carry out simple space and time computations.
(2) Quality: the swarm should be able to sense the quality change in the environment and response it.
(3) Diverse response: the swarm should not limit its way to get the resources in a narrow scope.
(4) Stability: the swarm should not change its behavior mode with every environmental change.
(5) Adaptability: the swarm should change its behavior mode when this change is worthy.

3.1.1 The purpose of PSO

The usual aim of the particle swarm optimization (PSO) algorithm is to solve an unconstrained minimization problem: find x* such that f(x*)<=f(x) for all d-dimensional real vectors x. The objective function f: R^d -> R is called the fitness function.

3.1.2 Basic description of PSO

PSO is a swarm intelligence meta-heuristic inspired by the group behavior of animals, for example bird flocks or fish schools. Similarly to genetic algorithms (GAs), it is a population-based method, that is, it represents the state of the algorithm by a population, which is iteratively modified until a termination criterion is satisfied. In PSO algorithms, the population P={p1,…,pn} of the feasible solutions is often called a swarm. The feasible solutions p1,…,pn are called particles. The PSO method views the set R d of feasible solutions as a "space" where the particles "move". For solving practical problems, the number of particles is usually chosen between 10 and 50.

3.1.3 Swarm topology

Each particle i has its neighborhood N_i (a subset of P). The structure of the neighborhoods is called the swarm topology, which can be represented by a graph. Usual topologies are: fully connected topology and circle topology.
Characteristics of particle i at iteration t:

- $x_i^{(t)}$: the position (a d-dimensional vector)
- $p_i^{(t)}$: the "historically" best position
- $l_i^{(t)}$: the historicaly best position of the neighboring particles; for the fully connected topology it is the historically best known position of the entire swarm
- $v_i^{(t)}$: the speed; it is the step size between $x_i^{(t)}$ and $x_i^{(t+1)}$

At the beginning of the algorithm, the particle positions are randomly initialized, and the velocities are set to 0, or to small random values. Parameters of the algorithm:

- $w^{(t)}$: inertia weight; a damping factor, usually decreasing from around 0.9 to around 0.4 during the computation
- φ_1, φ_2:acceleration coefficients; usually between 0 and 4.

3.1.4 Update of the speed and the positions of the particles

Many versions of the particle speed update exist, for example:

$$Vi^{t+1} = W^t Vi^t + \emptyset 1u1(Pi^t - Xi^t) + \emptyset 2u2(Ii^t - Xi^t) \quad (3.1)$$

The symbols u_1 and u_2 represent random variables with the U(0,1) distribution. The first part of the velocity formula is called "inertia", the second one "the cognitive (personal) component", the third one is "the social (neighborhood) component". Position of particle i changes according to

$$Xi^{t+1} = Xi^t + Vi^{t+1} \quad (3.2)$$

Stopping rule

The algorithm is terminated after a given number of iterations, or once the fitness values of the particles (or the particles themselves) are close enough in some sense.

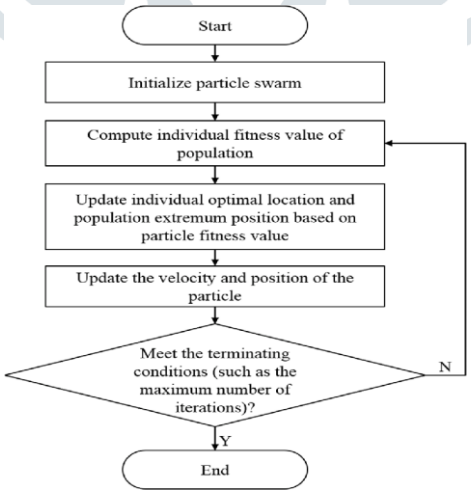

Figure 3.2 Flowchart of the PSO Algorithm

3.1.5 PSO variants

There is a plethora of different versions of PSOs, which usually modify the formula for the change of velocity (e.g., instead of u1 and u2 they use diagonal matrices U1 and U2, in other variants they use no inertia, but enforce an upper limit on the particle speed, there is the so-called "fully informed" PSO, and there is also a popular modification using a "constriction coefficient"). There exist versions of the PSO for constrained optimization, for discrete optimization, and for multi-objective optimization.

3.2 SYNCHRONOUS ROTATING REFERENCE FRAME-BASED PHASE-LOCKED LOOP (SRF-PLL)

The three-phase HBC is operated at grid-tied mode since the PV charging station needs ac grid as a backup supply. Integration of the three-phase HBC has to satisfy IEEE- 1547 standard which requires synchrony of the phase and angular

frequency of the three-phase HBC with the main grid [24], [25]. Synchronous rotating frame-based phase-locked loop (SRF-PLL) aligns the space vector of the point of common coupling (PCC) voltage to the d-axis and forces the q-axis PCC voltage V_{sq} to zero using a PI compensator as shown in Fig.3.3.

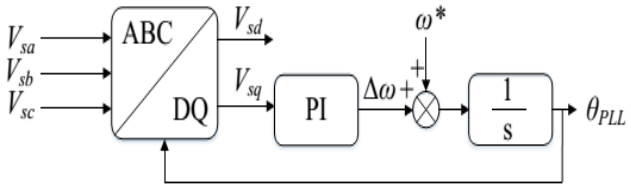

Figure 3.3 Basic schematic diagram of a SRF-PLL

$$Gpll = \frac{Kp,pll+Ki,pll}{S}\frac{S}{Vsd} \tag{3.2}$$

where $K_{p,PLL}$, $K_{i,PLL}$, and Vs are compensator parameters and the grid's voltage amplitude, respectively. The closed-loop transfer function of SRF-PLL is a second-order system with an oscillation mode with a damping factor ζ and a natural frequency ω_n. The parameters of the compensator are selected based on selecting ζ to be $1/\sqrt{2}$ while ω_n to be the reference frequency of the grid ω. The resulting parameters are:

$$Ki,pll = \frac{\omega^2}{Vs}, Kp,pll = \frac{2\zeta\sqrt{Ki,pll}}{Vs} \tag{3.3}$$

3.3 VECTOR CONTROL

Vector control technique is used for VSCs. The inner loop controls the ac current while the outer loop controls the dc voltage and reactive power. The dynamic equations of the three-phase HBC are similar to those of the conventional VSC examined in [26], [27]. The main difference of HBC is the consideration of D_{st}.

The inner current control loop is designed to respond much faster than the outer voltage controller for fast response and disturbance rejection. It is suggested to achieve fast transient response that the response of the inner loop to be in milliseconds, while the outer loop is 10 times slower than the inner loop. The open-loop of the inner current loop includes the transfer function of the plant and the delay of the modified PWM as well as the PI compensator.

$$Gi,ol(s) = \left(Kpi + \frac{Kii}{s}\right)\frac{1}{Lfs+Rf}\frac{1}{TpwmS+1} \tag{3.4}$$

where T_{PWM} is time delay of switching frequency of the modified PWM; K_{pi} and K_{pi} are the PI compensator's parameters for the inner current loop; L_f and R_f are the inductance and resistance filter components of the converter, respectively.

Tuning current compensator is achieved by using modulus optimum technique [27]. The concept of modulus optimum is defined as shifting the dominated poles that cause slow dynamic response and achieving unity gain for the closed-loop system. The PI controller's zero will cancel the pole dominated by the RL circuit dynamics. The open-loop transfer function becomes

$$Giol(s) = \frac{1}{S\,Tpwm(TpwmS+1)} \tag{3.5}$$

by choosing the following parameters:

$$Kpi = \frac{Lf}{Tpwm}, K_{ii} = \frac{Rf}{Tpwm}.$$

One of the advantage of the proposed HBC-based PV station is to generate a supported reactive power to the main grid. The controlling design of the reactive power loop is explained in details. The delivered reactive power of the HBC at PCC is calculated as:

$$Qpcc = \frac{-3}{2}Vsdi \tag{3.6}$$

where V_{sd} is the projection of the ac voltage component on d axis of the stationary reference frame; i_q is the projection of the output current of HBC on q reference frame. The open loop transfer function of the reactive power controller is given as follow:

$$Gol(s) = GQ(s)Gpi(s)Gsw(s)Gi(s)$$
$$Gol(s) = \left(\frac{3}{2}Vsd\right)\left(\frac{kpQS+kiQ}{S}\right)\left(\frac{1}{TpwmS+1}\right)\left(\frac{1}{LfS+Rf}\right) \tag{3.7}$$

where k_{pQ} and k_{iQ} are the PI compensator's parameters. Using modulus optimum technique on Equation (3.7), the open-loop and closed loop transfer functions of the reactive power equation are driven as:

$$Gol(s) = \frac{1}{\tau Qs(TpwmS+1)}$$
$$Gcl(s) = \frac{1}{Tpwm\tau Qs^2 + \tau Qs + 1}$$

$$kp = \frac{3}{2}\frac{Vsd\,Lf}{\tau Q}\ ; ki = \frac{3}{2}\frac{Vsd\,Rf}{\tau Q} \tag{3.8}$$

where τQ is the time constant of the resultant closed-loop system. Equation (3.8) represents a general form of the second order

system. The frequency of natural oscillation is obtained from (3.8) to be equal $\omega n = \sqrt{\frac{1}{Tpwm\ \tau Q}}$ while the damping factor equals $\varsigma = \sqrt{\frac{\tau Q}{4Tpwm}}$.

Assuming there is no switching power loss, the steady-state operation of power balance relationship of the three-phase HBC is given as:

$$Ppv = P\ cap + Pdc + Pac \tag{3.9}$$

$$Pac = \frac{3}{2}\ Vsd\ id \tag{3.10}$$

where i_d and V_{sd} are the projections of the ac current and grid voltage space vectors on the d-axis. The power relationship is further expressed as follows.

$$Pcap = CVdc = Ppv - Pac - Pdc$$
$$= Vdc\ Ipv - \frac{3}{2}Vsd\ id - Vdc\ Idc$$

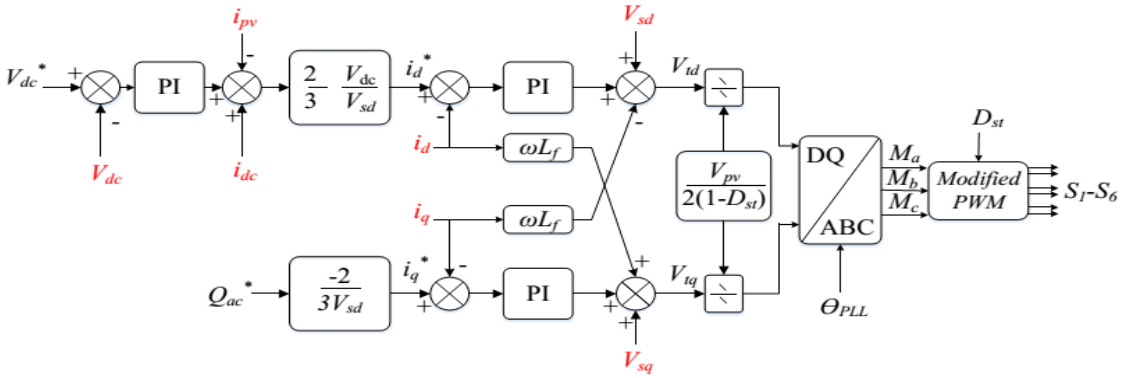

Figure 3.4 Vector control scheme of the three-phase HBC

Therefore, the dynamics of the capacitor voltage can be expressed as follows.

$$C\frac{dVdc}{dt} = Ipv - \frac{3}{2}\frac{Vsd}{Vdc}id - Idc = ud \tag{3.11}$$

A negative feedback controller will be designed to take in the dc voltage error $V_{dc}^* - V_{dc}$ and amplified by a PI controller. The output of the PI controller is ud. From this signal, the reference signal i^*_d will be generated as:

$$Id* = \frac{2}{3}\frac{Vdc}{Vsd}(ud - Ipv + Idc) \tag{3.12}$$

The open-loop transfer function of outer voltage is given as:

$$Gv,ol(s) = \left(Kpv + \frac{Kiv}{s}\right)\frac{1}{\tau is+1}\frac{1}{Cs} \tag{3.12}$$

where τ_i is the time constant for the inner current closed loop. The open-loop transfer function for voltage controller includes two poles at origin.

Symmetrical optimum is a technique to deal with an open loop system with double integrators [27]. The concept of symmetrical optimum is to operate the system at a low frequency to slow down the dynamic response which leads to an increased phase margin. The compensator parameters are given based on the symmetrical optimum method as follows:

$$Tiv = a^2 2\ \tau i\ , Kpv = \frac{C}{K\sqrt{Tiv}\sqrt{\tau i}}, Kiv = \frac{Kpv}{Tiv} \tag{3.13}$$

where K equals 3Vsd/2Vdc and a is the symmetrical frequency range between peak phase margin and low frequency operation area. It is important to select a high value of the symmetrical gain a to achieve high phase margin. The value of a falls between 2 and 4 [28].

IV. SIMULATION RESULTS

Case studies for a PV charging station using a three-phase HBC with the proposed control are conducted in MATLAB/SimPowerSystems environment. The system's parameters and PV data are given in Table I. The data for the PV model are based on PV array type Sunpower SPR-E20-327.

The battery parameters of Chevrolet Volt and Nissan Leaf are used to represent the batteries of PHEVs [7], [29], [30]. Two case studies are conducted to evaluate MPPT and vector control as well as to illustrate the operation modes of the PV charging station.

4.1 CASE 1: PERFORMANCE OF THE PSO - MPPT

The goal of this case study is to validate the performance of the modified MPPT using incremental conductance-PI algorithm. Fig.4.1 shows the performance of MPPT when the system is subject to solar irradiance variation.

The dc voltage V_{dc} and the PV voltage V_{pv} are related based on the duty cycle ratio D_{st} that is generated from MPPT. The role of vector controller is to keep the dc voltage V_{dc} at its reference value 350V and supply reactive power Q^*_{ac} to the ac grid. The role of MPPT algorithm is to adjust the duty cycle ratio D_{st} and in turn adjust the PV output voltage V_{pv} so that the PVs are operating at the maximum power extracting point.

Table 4.1 system parameters

	PARAMETER		PARAMETER
PV	V_{oc} =65.1V V_{mpp} =54.7V I_{sc} =6.46A I_{mpp} =5.98A R_{sh} =298.531Ω R_s =0.369Ω	AC	$V_{grid\ (L-L)}$ = 20Kv ω = 377rad/s S =100kVA $V_{t(L-L)}$ =208V R_f =2mΩ L_f =125μH C_f =150μF
DC	V_{dc} =350V L =5mH Load =100kV L_{dc} =10mH C_{dc} =100μF	Control	K_{pi} =0.625Ω K_{ii} =10Ω/s K_{pv} =0.24$Ω^{-1}$ K_{iv} =300$Ω^{-1}$/s K_{pvdc} =0.001 K_{ivdc} =25 K_{iidc} =0.001 K_{iidc} =3
Chevy	# of cells:200 V_{cell} =1.25V $Q_{energ\ y}$=16kWh Type :Li-Ion	Nissan	# of cells:160 V_{cell} =1.875V Q_{energy} =24kWh Type :Li-Ion

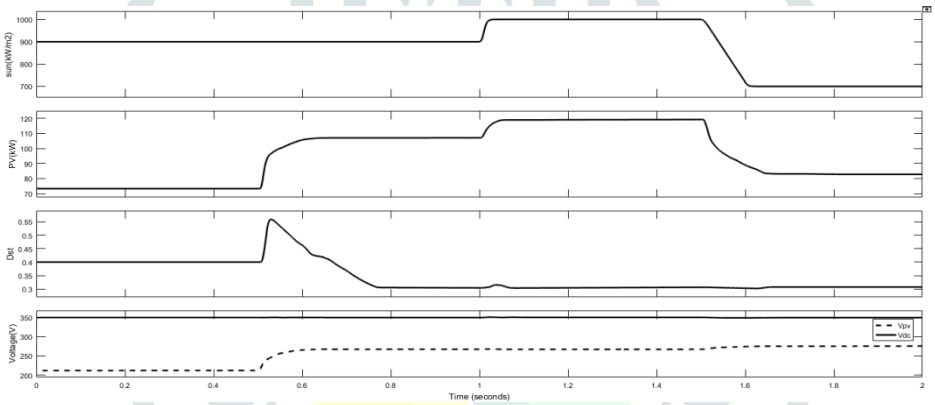

Figure 4.1 Performance of PSO-MPPT when sun irradiance variation is applied

Fig.4.1 provides the performance of MPPT based on four different intervals. From 0− 0.5 seconds, the sun irradiance is 0.9 kW/m2 and the MPPT control is not activated. The output PV power supplies approximately 70 kW. At t = 0.5 seconds, MPPT is activated, the duty cycle ratio is decreased and the PV voltage is improved. This in turn improves the PV power output to be 90 kW. Note that whether the MPPT is on or off, V_{dc} is kept at 350 V.

At t=1 second and t=1.5 seconds, the sun irradiance increases and decreases. Due to the MPPT control, the optimal PV output voltage is kept at the optimal level. Further, the PV output power tracks the maximum point at each irradiance level.

Fig.4.1 validates the good tracking performance of MPPT when different solar irradiations are applied to the PV. The simulation results also show that the vector controller can regulate the dc voltage at 350 V and reject disturbances.

4.2 CASE 2: POWER MANAGEMENT OF THE PV CHARGING STATION

An objective of the three-phase HBC is to charge PHEVs even when there is not enough PV power. The performance of the PV charging station is evaluated when different values of solar irradiation are applied. The main goal of this case study is to show continuous charging PHEVs even when the PV power is low. At day time the solar irradiance is assumed to be 1 kW/m^2 while at sun set the irradiance decreases to 0.7 kW/m^2.

The dc load first consumes 50 kWh which represents charging of two Nissan Leaf vehicles. The two Nissan Leafs are charged before the PV power decreases as shown in Fig.4.2. The remaining of PV power transfers to the main grid. At t = 0.5 seconds, the PV power reduces due to irradiance change. Two more vehicles are connected to the system consequently at t = 1 seconds and t = 1.5 seconds. Fig.4.2 shows that the PV array can provide power to the third car at t = 1.5 seconds. The PV power is used to charge the batteries of PHEV with no dependency on the main grid.

At t = 1.5 seconds, the fourth electric car (Chevy Volt 2) is connected to the system. The bidirectional feature of the three phase HBC and the regulated dc voltage controller allow the dc load to absorb power from the main grid to charge the fourth vehicle. It is also noticed that the three phase HBC can achieve power balance as well as maintain constant dc voltage at 350V.

Fig.4.2 also shows that the reactive power Q_{ac} is kept at 0. This shows that the three-phase HBC can achieve decoupled control of real and reactive power. Fig.4.3 presents the duty cycle ratio and the modulation index in dq-axes.

This case study demonstrates that the proposed control can provide smooth transition when HPEVs are connected into the PV charging station.

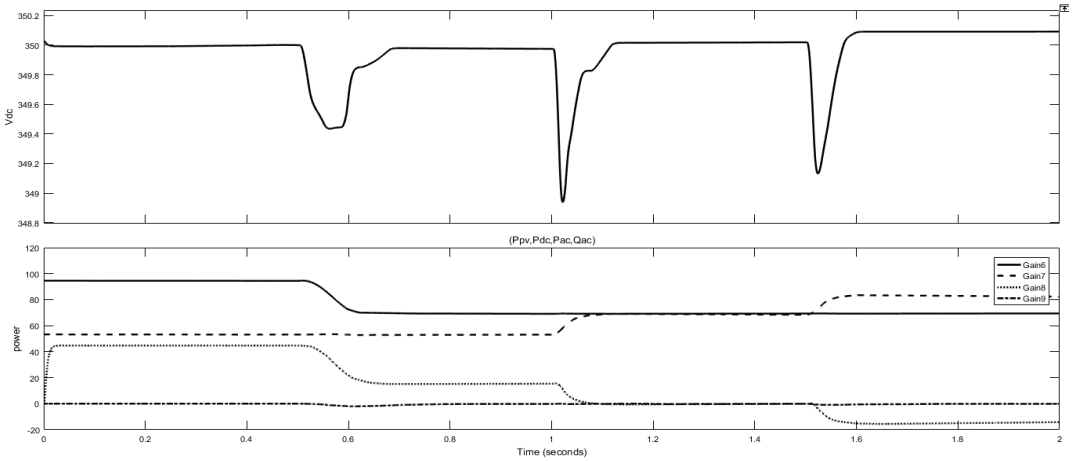

Figure 4.2 Power management of a charging station

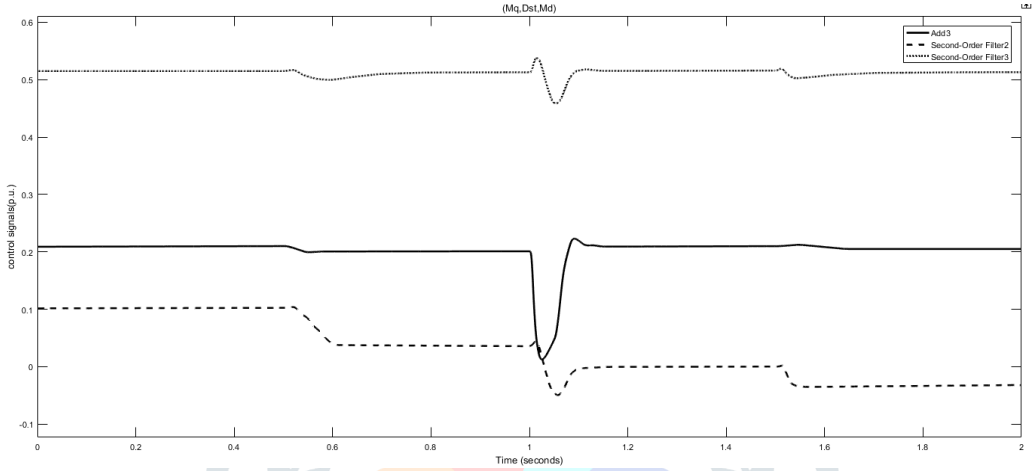

Figure 4.3 Mq, Dst and Md

V. CONCLUSION

Control of three-phase HBC in a PV charging station is proposed in this paper. The three-phase HBC can save switching loss by replacing a dc/dc boost converter and a dc/ac converter into a single converter structure.

A new control for the three-phase HBC is designed to achieve MPPT and power management called Particle Swarm Optimisation based MPPT method. This method can be applied to optimization problems of large dimensions, often producing quality solutions more rapidly than alternative methods. The PSO algorithm maintains multiple potential solutions at one time.

Two case studies are conducted in MATLAB simulation to demonstrate the performance of MPPT, and overall power management of the PV charging station. The simulation results show the effectiveness and robustness of the proposed control for PV charging station to maintain continuous dc power supply using both PV power and ac grid power to PHEV's.

REFERENCES

[1] Ahmad Tazay, Zhixin Miao, Control of a Three-Phase Hybrid Converter for a PV Charging Station , 2018,IEEE.
[2] M. Ehsani, Y. Gao, and A. Emadi, Modern electric, hybrid electric, and fuel cell vehicles: fundamentals, theory, and design. CRC press, 2009.
[3] K. Sikes, T. Gross, Z. Lin, J. Sullivan, T. Cleary, and J. Ward, "Plug- in hybrid electric vehicle market introduction study: final report," Oak Ridge National Laboratory (ORNL), Tech. Rep., 2010.
[4] A. Khaligh and S. Dusmez, "Comprehensive topological analysis of con- ductive and inductive charging solutions for plug-in electric vehicles," IEEE Transactions on Vehicular Technology, vol. 61, no. 8, pp. 3475– 3489, 2012.
[5] T. Anegawa, "Development of quick charging system for electric vehi- cle," Tokyo Electric Power Company, 2010.
[6] F. Musavi, M. Edington, W. Eberle, and W. G. Dunford, "Evaluation and efficiency comparison of front end ac-dc plug-in hybrid charger topologies," IEEE Transactions on Smart grid, vol. 3, no. 1, pp. 413– 421, 2012.
[7] M. Yilmaz and P. T. Krein, "Review of battery charger topologies, charging power levels, and infrastructure for plug-in electric and hybrid vehicles," IEEE Transactions on Power Electronics, vol. 28, no. 5, pp. 2151–2169, May 2013.
[8] G. Gamboa, C. Hamilton, R. Kerley, S. Elmes, A. Arias, J. Shen, andBatarseh, "Control strategy of a multi-port, grid connected, direct-dc pv charging station for plug-in electric vehicles," in Energy Conversion Congress and Exposition (ECCE), 2010 IEEE. IEEE, 2010, pp. 1173– 1177.
[9] P. Goli and W. Shireen, "Pv integrated smart charging of phevs based on dc link voltage sensing," IEEE Transactions on Smart Grid, vol. 5, no. 3, pp. 1421–1428, 2014.
[10] S. Mishra, R. Adda, and A. Joshi, "Inverse watkins–johnson topology- based inverter," IEEE Transactions on Power Electronics, vol. 27, no. 3, pp. 1066–1070, 2012.
[11] O. Ray and S. Mishra, "Boost-derived hybrid converter with simulta- neous dc and ac outputs," IEEE Transactions on Industry Applications, vol. 50, no. 2, pp. 1082–1093, March 2014.
[12] O. Ray, V. Dharmarajan, S. Mishra, R. Adda, and P. Enjeti, "Analysis and pwm control of three-phase boost-derived hybrid converter," in 2014 IEEE Energy Conversion Congress and Exposition (ECCE), Sept 2014, pp. 402–408.

[13] O. Ray and S. Mishra, "Integrated hybrid output converter as power router for renewable-based nanogrids," in Industrial Electronics Society, IECON 2015 - 41st Annual Conference of the IEEE, Nov 2015, pp. 001 645–001 650.
[14] M. A. Elgendy, B. Zahawi, and D. J. Atkinson, "Assessment of perturb and observe mppt algorithm implementation techniques for pv pumping applications," IEEE transactions on sustainable energy, vol. 3, no. 1, pp. 21–33, 2012.
[15] J. Khazaei, Z. Miao, L. Piyasinghe, and L. Fan, "Real-time digital simulation-based modeling of a single-phase single-stage pv system," Electric Power Systems Research, vol. 123, pp. 85–91, 2015.
[16] M. Tabari and A. Yazdani, "Stability of a dc distribution system for power system integration of plug-in hybrid electric vehicles," IEEE Transactions on Smart Grid, vol. 5, no. 5, pp. 2564–2573, 2014.
[17] O. Ray and S. Mishra, "Integrated hybrid output converter as power router for renewable-based nanogrids," in Industrial Electronics Society, IECON 2015-41st Annual Conference of the IEEE. IEEE, 2015, pp. 001 645–001 650.
[18] U. Eicker, Solar technologies for buildings. John Wiley & Sons, 2006.
[19] N. Femia, G. Petrone, G. Spagnuolo, and M. Vitelli, Power electronics and control techniques for maximum energy harvesting in photovoltaic systems. CRC press, 2012.
[20] M. R. Patel, Wind and solar power systems: design, analysis, and operation. CRC press, 2005.
[21] O. Ellabban, J. V. Mierlo, and P. Lataire, "Comparison between different pwm control methods for different z-source inverter topologies," in Power Electronics and Applications, 2009. EPE '09. 13th European Conference on, Sept 2009, pp. 1–11.
[22] T. Esram, P. L. Chapman et al., "Comparison of photovoltaic array maximum power point tracking techniques," IEEE Transactions on Energy Conversion EC, vol. 22, no. 2, p. 439, 2007.
[23] C. Dorofte, U. Borup, and F. Blaabjerg, "A combined two-method mppt control scheme for grid-connected photovoltaic systems," in Power electronics and applications, 2005 European conference on. IEEE,2005, pp. 10–pp.
[24] "Ieee standard for interconnecting distributed resources with electric power systems," IEEE Std 1547-2003, pp. 1–28, July 2003.
[25] D. Dong, B. Wen, D. Boroyevich, P. Mattavelli, and Y. Xue, "Analysis of phase-locked loop low-frequency stability in three-phase grid-connected power converters considering impedance interactions," IEEE Transactions on Industrial Electronics, vol. 62, no. 1, pp. 310–321, Jan 2015.
[26] A. Yazdani and R. Iravani, Voltage-sourced converters in power systems: modeling, control, and applications. John Wiley & Sons, 2010.
[27] A. Tazay, Z. Miao, and L. Fan, "Blackstart of an induction motor in an autonomous microgrid," in 2015 IEEE Power Energy Society General Meeting, July 2015, pp. 1–5.
[28] F. Fr¨ohr and F. Orttenburger, Introduction to electronic control engineering. Heyden, 1982.
[29] N. Leaf, "2011 leaf owner's manual revised," 2011. [Online]. Available: http://www.nissan-techinfo.com/refgh0v/og/leaf/2011-nissan-leaf.pdf
[30] G.Motors," 2016 chev rolet volt battery system,"2016[Online].Available: https://media.gm.com/content/dam/Media/microsites/product/Volt2016/doc/VOLT_BATTERY.pdf